Transp Porous Med
DOI 10.1007/s11242-009-9456-4

Flux in Porous Media with Memory: Models and Experiments

Erika Di Giuseppe · Monica Moroni · Michele Caputo

Received: 22 January 2009 / Accepted: 17 July 2009

Abstract The classic constitutive equation relating fluid flux to a gradient in potential (pressure head plus gravitational energy) through a porous medium was discovered by Darcy in the mid 1800s. This law states that the flux is proportional to the pressure gradient. However, the passage of the fluid through the porous matrix may cause a local variation of the permeability. For example, the flow may perturb the porous formation by causing particle migration resulting in pore clogging or chemically reacting with the medium to enlarge the pores or diminish the size of the pores. In order to adequately represent these phenomena, we modify the constitutive equations by introducing a memory formalism operating on both the pressure gradient–flux and the pressure–density variations. The memory formalism is then represented with fractional order derivatives. We perform a number of laboratory experiments in uniformly packed columns where a constant pressure is applied on the lower boundary. Both homogeneous and heterogeneous media of different characteristic particle size dimension were employed. The low value assumed by the memory parameters, and in particular by the fractional order, demonstrates that memory is largely influencing the experiments. The data and theory show how mechanical compaction can decrease permeability, and consequently flux.

Keywords Porous media · Memory's formalism · Fractional derivatives · Mechanical compaction

E. Di Giuseppe
Laboratoire FAST, Bât. 502, Campus Universitaire Orsay, F91405 Orsay, France

M. Moroni (✉)
Department of Hydraulics, Transportations and Roads, Sapienza University of Rome, via Eudossiana 18, 00184 Rome, Italy
e-mail: monica.moroni@uniroma1.it

M. Caputo
Department of Physics "G. Marconi", Sapienza University of Rome, Piazzale A. Moro 5, 00185 Rome, Italy

Published online: 23 August 2009

1 Introduction

Flow through porous media is a subject of interest in many branches of science, i.e., hydrogeology, chemical engineering, and in the field of petroleum extraction. The investigation of its features plays a major role in the comprehension of many phenomena, as the subsidence caused by water shortage, or the process of crystallization of the ores in a well thermal exit, which makes them unusable for the extraction of the heat. Moreover, it is important to investigate both the correlation between sismogenesis and the introduction of fluids in the subsoil, studied in the Rangeley Colorado experiment (Raileigh et al. 1976), and the link between the increase in the seismic activity and the growth of the water level in wells (Bell and Nur 1978).

Researchers are focusing on developing relations between piezometric pressure gradient, macroscale geometry properties of the medium, thermophysical properties of both medium and fluid, and the fluid velocity field relative to the solid matrix (Wang 2000). The macro or Darcy scale is employed in this analysis. At this scale, Darcy's law establishes a linear relation between the pressure gradient and the fluid velocity field with the proportional coefficient (hydraulic conductivity) depending on the thermophysical properties of both medium and fluid (Bear 1972; Scheidegger 1960). It has been experimentally verified (Elias and Hajash 1992; Bell and Nur 1978; Roeloffs 1988) that when a fluid flows through a porous medium, the permeability of the matrix may be locally variable in time (Caputo 2000; Iaffaldano et al. 2006; Cloot and Botha 2006) for several reasons, i.e., chemical dissolution of the medium, swelling and flocculation, pore plugging and precipitation reactions, transport of particles obstructing the pores, mechanical compaction, and grain crumbling due to high pressure occur (Bell and Nur 1978; Caputo 1999). Mechanical compaction and crumbling can also simultaneously act. Crumbling provides new material for compaction, which rearranges grains creating favorable conditions for further crumbling. All these phenomena, in conjunction with possible chemical reactions between the fluid and the medium, create continuous local changes of both porosity resulting in memory, i.e., at a given instant of time the advection process is affected by the history of pressure and flux (Iaffaldano et al. 2006). Thereby, the governing equations of advection present analytical difficulties because the variation of the permeability is not known a priori (Caputo and Plastino 2004).

In general, the terms "convection," "advection," and "diffusion" are interchangeably used to describe the flux of a fluid in a porous medium, but they also assume different meanings in Physics, in Engineering, or in Earth Science. Therefore, to avoid confusion, in this article only the term "advection" is used.

Many researchers have attempted to extend Darcy's law but, because of the complexity of the problem, initial attempts have relied on models of intuitive or empirical nature (Kaviany 1995). More systematic theoretical approaches developed include macroscale local models, i.e., mixture theory, local volume-averaging and hybrid mixture theory (for a nice review see Wang 2000), and macroscale non-local models suitable for describing the macroscale fluid transport, which is affected by phenomena taking place in a hierarchy of spatial scales (Cushman 1997). Neuman (1993) derived the exact non-local (integro-differential) equations for the mean and variance–covariance of transformed head and flux rate, conditioned on measured values of log conductivity for transient flow in bounded, randomly heterogeneous porous media. Singh et al. (2003, 2004) developed a non-local continuum thermodynamics-based approach applicable to biopolymers to include the effects of some multiscale phenomena on macroscale fluid transport. In the model proposed here, fractional order derivatives are introduced to rewrite the constitutive equations with a memory formalism (Caputo 2000) and account for the non-local aspects of fluid transport. While only one parameter historically is

introduced in Darcy's law to relate the pressure gradient and the fluid velocity field, the flux rate here depends on the fractional derivative order and on an additional number of parameters (the memory parameters) mathematically describing the changes of both solid matrix and fluid characteristics due to crumbling, mechanical compacting, and chemical reactions. Experiments validate this generalized theory.

In the last 30 years, the use of the fractional derivatives to mimic the effects of the memory is largely used in electromagnetism (Jacquelin 1984), biology (Cesarone 2002), chaos (e.g., Mainardi 1996), economy (e.g., Caputo and Kolari 2001), and the rheology properties of solids (Le Mehaute and Crepy 1983; Bagley and Torvik 1986; De Espindola et al. 2005; Adolfsson et al. 2005). Concerning this last point, lately the memory, i.e., the history of the deformation and fractures of a solid under stress, is largely used. In fact, the propagation of a fracture within a solid is the effect of the memory (e.g., Christensen 2003).

Moreover, they have also been used to describe the dissipative properties of materials (Caputo and Mainardi 1971): to show the constitutive equation of polarizable media (Caputo and Plastino 1998); to modify Fick's law to take into account non-local phenomena in turbulent transport modeling (Paradisi et al. 2001); to modify Fick's law to describe the passive diffusion process across two different membrane systems, i.e., a biological membrane (Cesarone et al. 2005); to describe stochastic processes in statistical finance assuming that not only prices can be modeled as random variables but also that time between two consecutive transactions vary in a stochastic fashion (Mainardi et al. 2000; Scalas et al. 2000; Caputo 2002); to provide a general approach to fractional calculus as simple as possible for topics concerning either relaxation and oscillations, or diffusion and wave propagation (Mainardi 1996). In a recent study by Iaffaldano et al. (2006), the constitutive equations of advection have been rewritten to provide a memory model for advection of water in porous media. Their proposed model fits well the flux rate observed in experiments of water flux through sand. In order to simplify the computation, only the transient phase has been studied, and the parameter describing the asymptotic value has been set equal to zero.

The use of the memory formalism, and consequently of fractional derivatives, comes out to be very useful.

In our study, we assumed the definition of fractional derivatives formulated by Caputo (1969, 2000). However, other definitions of non-integer derivatives do exist.

A larger number of laboratory experiments have been performed, by using different particle size sands and pressure, to investigate how different conditions may affect the memory. Moreover, the number of the memory's parameters has been increasing so that the computations are able to provide quantitatively also the asymptotic value of the flux. A good agreement has been obtained between the variations in time of both the theoretical and the observed flow.

The derivative of fractional order is introduced in Sect. 2 as well as the theoretical model describing the flux of a fluid through a porous medium when a constant pressure is applied to both boundaries. The dependence of flux rate from the model parameters and the procedure of fitting data are described in Sect. 3. The experimental setup providing data to test the theory is described in Sect. 4. Section 5 presents the data and the results of the application of the adaptation procedure, and Sect. 6 concludes the article with discussion and conclusions.

2 The Theory

The three constitutive equations of the classical theory of advection state are as follows:

$$q = -D\nabla p \tag{1.a}$$

$$p = Gm \tag{2.a}$$

$$\frac{\partial m}{\partial t} + \nabla \boldsymbol{q} = 0 \tag{3}$$

where $\boldsymbol{q}$ is the flux rate, D is the Darcy coefficient depending on both the porous matrix and the fluid phase characteristics, m is the fluid mass per unit volume, and p is pressure. Equation 3 represents the continuity equation.

We will use a constitutive equation containing a memory formalism to replace the classic Darcy's law as follows (Caputo 2000; Caputo and Plastino 2004; Iaffaldano et al. 2006):

$$f_1(t) * \boldsymbol{q} = -f_2(t) * \nabla p \tag{1.b}$$

where the symbol * indicates the convolution product, and $f_1(t)$ and $f_2(t)$ are integro-differential operators.

As we consider both the fluid and the porous matrix to be subject to changes of their physical properties, the relation between the variation of the fluid mass per unit volume, m, and the pressure, p, may be modified as well:

$$\varphi_1(t) * p = \varphi_2(t) * m \tag{2.b}$$

where $\varphi_1(t)$ and $\varphi_2(t)$ are integro-differential operators.

All integro-differential operators, introduced in the previous equations, represent the local variations that are due to temperature changes and/or chemical and physical interactions of the fluid with the matrix.

We define the integro-differential operators in (1.b) and (2.b) as follows:

$$f_1(t) = \gamma\delta(t) + \varepsilon t^{-n_1} \frac{\partial}{\Gamma(1-n_1)\partial t} \tag{4a}$$

$$f_2(t) = c\delta(t) + d t^{-n_2} \frac{\partial}{\Gamma(1-n_2)\partial t} \tag{4b}$$

$$\varphi_1(t) = a\delta(t) + b t^{-m_1} \frac{\partial}{\Gamma(1-m_1)\partial t} \tag{4c}$$

$$\varphi_2(t) = \alpha\delta(t) + \beta t^{-m_2} \frac{\partial}{\Gamma(1-m_2)\partial t} \tag{4d}$$

where $\delta(t)$ is the delta of Dirac function, Γ is the Euler Γ function; $0 \le n_1 < 1$, $0 \le n_2 < 1$, $0 \le m_1 < 1$, and $0 \le m_2 < 1$; $a, b, c, d, \alpha, \beta, \gamma$, and ε are the so called "memory parameters," and their dimension in c.g.s. units are: $a[s^2 cm^{-2}]$, $b[s^{2+n} cm^{-2}]$, $c[s^n]$, $d[s^{1+n}]$, $\alpha[1]$, $\beta[s^n]$, $\gamma[1]$, and $\varepsilon[s^n]$ (Caputo 2000).

Using the expressions above for $f_1(t)$, $f_2(t)$, $\phi_1(t)$, ϕ_2(t), and recalling

$$f(t) * g(t) = \int_0^t f(t-\tau) g(\tau) d\tau$$

Equations 1.b and 2.b are modified as follows:

$$\left(\gamma + \varepsilon \frac{\partial^{n_1}}{\partial t^{n_1}}\right) \boldsymbol{q} = -\left(c + d \frac{\partial^{n_2}}{\partial t^{n_2}}\right) \nabla p \tag{5}$$

$$\left(a + b \frac{\partial^{m_1}}{\partial t^{m_1}}\right) p = \left(\alpha + \beta \frac{\partial^{m_2}}{\partial t^{m_2}}\right) m \tag{6}$$

Fractional order derivatives have been introduced by using Caputo's definition (Caputo 2000; Podlubny 1999):

$$f^{(n)}(t) = \frac{\partial^n f(t)}{\partial t^n} = \frac{1}{\Gamma(1-n)} \int_0^t \frac{\dot{f}(\tau)}{(t-\tau)^n} d\tau$$

where $0 \leq n < 1$. The "weight function" is

$$j(t) = t^{-n} / \Gamma(1-n)$$

In the special case of $n = 0$, $\Gamma(1) = 1$, and $j(t) = 1$, the weights are constant, i.e., the index n is a gauge of shortness for the memory in $f^{(n)}(t)$ relative to $f(t)$.

Thus, the physical content of the Darcy's law is affected by its generalized version, showed in (7). The classical Darcy's law satisfies the principal of local action, i.e., the flow is directly influenced by its immediate surrounding. Thus, the fluid flux is just given by the values of the pressure gradient and the permeability at the specific point under consideration. The use of the memory formalism changes this postulate. We assume that the flow in a porous medium still depends not only on the pressure head at a specific time (space), but also on its history. The "weight function" in the integration process takes into account that the variations of the fluid flow are primarily controlled by local processes, and less by far-field values.

One should note that more than one parameter has been employed to describe the flux of the fluid through the porous medium. The memory's formalism implies the use of nine parameters $a, b, c, d, \alpha, \beta, \gamma, \varepsilon$, and n, instead of the single parameter $k\rho g/\mu$ on which the classic Darcy's law is based. The large number of the parameters allows the investigation of several different models to describe advection with memory.

In order to solve the previous equations, initial and boundary conditions must be applied. We assume the porous medium to be homogeneous and of finite thickness h. A constant pressure is applied to both the medium boundaries with a larger value applied to the lower boundary. Finally, we assume the flow to take place along the z direction (positive downward and with the origin located at the medium upper boundary), and the associated flux rate to be $q(z, t)$.

The equations in the Laplace domain are:

$$(\gamma + \varepsilon s^{n_1}) Q(z,s) = -(c + d s^{n_2}) P_z(z,s) \tag{7}$$

$$(a + b s^{m_1}) P(z,s) - b s^{m_1 - 1} p(z,0) = (\alpha + \beta s^{m_2}) M(z,s) - \beta s^{m_2 - 1} m(z,0) \tag{8}$$

$$Q_z(z,s) + s M(z,s) - m(z,0) = 0 \tag{9}$$

where s is the Laplace variable, and the initial flux and the pressure gradient are set to zero. Q, Q_z, P, P_z, and M are the Laplace transforms of respectively $q(z,t)$, $\frac{\partial q(z,t)}{\partial z}$, $p(z,t)$, $\frac{\partial p(z,t)}{\partial z}$, and $m(z,t)$.

Equation 9 is solved in terms of $M(z,s)$ and inserted into (8). In the new equation, the result of the differentiation of (7) with respect to z is substituted to obtain a second-order non-homogeneous differential equation. Solving this differential equation and substituting $P_z(z,s)$ in (7), we obtain the explicit expression of $Q(z,s)$. All the intermediate equations are described in explicit form in the Appendix.

In order to reduce the number of memory parameters and to simplify formulas, **we** assume that $n_1 = n_2 = m_1 = m_2 = n$. We further impose $b = \beta = 0$, to neglect fluid rheology and assume a direct proportionality between fluid pressure and the variation of fluid mass per unit volume. For simplicity, we look at the limit as $\varepsilon \to 0$. Thereby, these assumptions imply that the memory is only in Eq. 7.

The memory in this model implies physically consistent filtering mechanisms (Caputo 2001). In fact, this memory formalism can also model the dispersion and the dissipation in dielectric and anelastic media, by assuming that m and q substitute the induction (deformation) and p and ∇p the applied electric field (stress) (Caputo and Mainardi 1971).

In addition, it is possible to investigate the effects of the memory only due to the fluid rheology, for example, by setting $\varepsilon = d = 0$. In this case, all the terms including the fractional derivatives in Eq. 7 are neglected, whereas the memory dependency between the pressure and the variation of the mass per unit volume is considered. The variability of different models has been extensively investigated in Caputo (2000) and Caputo and Plastino (2004).

In the Laplace domain, the flux presents then the following expression:

$$Q(z,s) = -\frac{K}{s}\left[\frac{a}{\alpha\gamma}s(c+ds^n)\right]^{1/2}\left[\frac{e^{M(z-h)}+e^{-M(z-h)}}{e^{Mh}-e^{-Mh}}\right] \tag{10}$$

where M is defined in the Appendix, and K is the pressure applied to a lower boundary of the porous medium.

This function has a first order pole at $s = 0$ (the "extreme value theorem" (EVT) can be applied here)

$$\lim_{s\to 0} sQ(0,s) = \lim_{t\to\infty} q(0,t) = -\frac{Kc}{h\gamma}$$

This limit is, also, the residuum of the flux function.

Substituting appropriately parameters and setting $s = re^{i\pi}$ to calculate the Laplace anti-transform in the complex plane (Iaffaldano et al. 2006), we obtain, for the flux in real space and time, the following expression:

$$\begin{aligned} q(z,t) = -\frac{K}{2\pi}\int dre^{-rt}\rho\left(\frac{A}{r}\right)^{1/2}\Bigg\{&(\cos\varphi + i\sin\varphi)\left[\frac{e^l(v+io)+e^{-l}(v-io)}{e^u(y+iw)-e^{-u}(y-iw)}\right] \\ &+(\cos\varphi - i\sin\varphi)\left[\frac{e^{-l}(v+io)+e^l(v-io)}{e^u(y-iw)-e^{-u}(y+iw)}\right]\Bigg\} \end{aligned} \tag{11}$$

where $A = a/\alpha$, $v = \cos((z-h)C\cos\varphi)$, $o = \sin((z-h)C\cos\varphi)$, $y = \cos(hC\cos\varphi)$, $w = \sin(hC\cos\varphi)$, $l = (z-h)C\sin\varphi$, $u = hC\sin\varphi$, $\varphi = \frac{1}{2}arctg\left[\frac{Dr^n\sin(n\pi)}{B+Dr^n\cos(n\pi)}\right]$, $B = c/\gamma$, $D = d/\gamma$, $\mathrm{C} = (Ar)^{1/2}/\rho$, $\rho = [B^2 + 2BDr^n\cos(n\pi) + (Dr^n)^2]^{1/4}$.

In particular, the inverse Laplace transform (TL^{-1}) of $Q(0,s)$ provides the flux $q(0,t)$ at the medium upper boundary $z = 0$:

$$q(0,t) = TL^{-1}[Q(0,s)] = -K\left[\frac{1}{2\pi}\int_0^{+\infty} e^{-rt}\left(\frac{A}{r}\right)^{1/2}\rho\frac{NUM(r)}{DEN(r)}dr + \frac{B}{h}\right] \tag{12}$$

where the numerator NUM(r) and the denominator DEN(r) are real and they are equal to

$$\begin{aligned} \mathrm{NUM}(r) = \;& 2\cos\varphi[(vy+ow)(\mathrm{e}^{l+u}-\mathrm{e}^{-l-u})+(vy-ow)(\mathrm{e}^{u-l}-\mathrm{e}^{l-u})] \\ & -2\sin\varphi[(oy-vw)(\mathrm{e}^{l+u}+\mathrm{e}^{-l-u})-(vw+oy)(\mathrm{e}^{l-u}+\mathrm{e}^{u-l})] \\ \mathrm{DEN}(r) = \;& (y^2+w^2)(\mathrm{e}^{2u}+\mathrm{e}^{-2u})-2(y^2-w^2) \end{aligned}$$

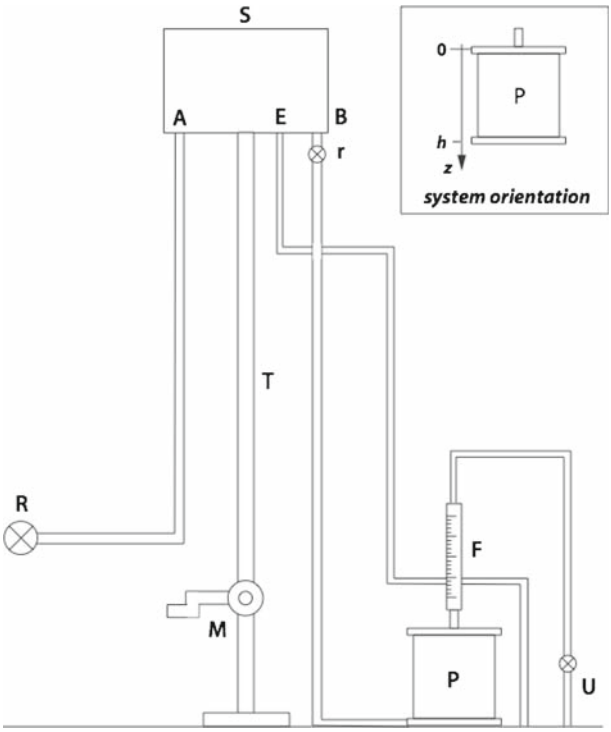

Fig. 1 Scheme describing the experimental setup. In the small panel the reference system orientation is shown

3 Experimental Set-Up and Procedures

Several experiments in a one-dimensional (1-D) flow field were performed to determinate the flow rate through a uniformly packed column of porous media filling a constant head permeameter. The experimental setup was designed on purpose to determine the memory parameters appearing within the equations (par. 2) describing the instantaneous flux rate through a porous medium layer when a constant pressure is applied on the medium lower boundary (Fig. 1).

Water was used as the fluid phase.

3.1 Apparatus

The experimental apparatus, allowing a constant pressure to be applied at the lower boundary of the porous medium, is composed of a tank to store water, a permeameter to contain the porous matrix, a rotameter to measure the flow rate, and several handles and tubes to control and eventually interrupt the flux through the medium. The hydraulic circuit is presented in Fig. 1 along with the 1-D, reference system oriented along the permeameter axis, positive downward.

The permeameter (P) consists of an aluminum empty cylinder of 10-cm inner diameter suitable for containing the porous matrix.

The inlet and outlet permeameter boundaries are separated from the porous medium by thin nylon meshes with hydraulic conductivity larger than the samples. The permeameter

is fed by the fluid phase from the bottom ($z = h$) to the top ($z = 0$) through the tube (T) connected to a parallelepiped constant head tank (S; $32 \times 21 \times 26.5\text{cm}^3$). An on–off tap ($B$) allows the tank and the permeameter to be disconnected. Water exceeding the fixed height within the tank is collected as surplus water in a second sector within the tank and evacuated through the tube (E). This ensures that a constant pressure is maintained at the lower boundary plane $z = h$. The tank is mounted on a moving stage. The handle (M) allows the height of the tank (h_{tank}) to be adjusted to the one required for the experiment. In time dependent pressure experiments, which are not presented here, the height of the tank may be varied over time. The upper boundary of the permeameter ($z = 0$) is connected to a rotameter for measuring instantaneous values of the flow rate. The rotameter scale ranges from 65 to 680 l/h with an error of 5 l/h.

The cylinder axis is vertical, whereas in Iaffaldano et al. (2006) experiments, the permeameter axis was horizontal. In a three-dimensional flow configuration, gravity has to be accounted for. In fact, the vertical pressure drop, due to the gravity, can affect the flow. Hence, the Darcy's law showed in the Eq. 1.b should have the following expression:

$$f_1(t) * \boldsymbol{q} = f_2(t) * \nabla H$$

where H is the hydraulic head, and it is equal to $(z + p/\rho g)$.

In our theoretical flux rate derivation, the term describing the gravitational pressure drop, z, was neglected. This is reasonable if the gradient $\partial p/\partial z$ is much larger than 1. By assuming that the pressure changes linearly between the boundaries of the permeameter and making the proper substitution, we find $\partial p/\partial z$ results to be proportional to the ratio of the tank height, h_{tank}, and the porous sample height, h. As h_{tank} is $\sim$2 m and h is $\sim$0.1 m, the ratio is much larger than 1. Hence, z can be neglected, and it is reasonable to use the Darcy's law in the form shown by Eq. 1.b, as Iaffaldano et al. (2006) did in their models. The accuracy of the theoretical flux is 5%.

3.2 Porous Media

Six porous media were investigated: five kinds of sand of different particle size distribution and Pyrex cylinders of 7-mm mean length and 3-mm diameter. In order to distinguish different experiments the following nomenclature has been adopted: Homo1, Homo2, and Homo3 refer to three types of sands with an almost uniform particle size distribution (Fig. 2a, b, their grain size weighted mean values being, respectively, 0.16, 0.17, and 0.25 mm); Heter1 and Heter2 refer to two types of sands with a graded particle size distribution (Fig. 2a, the grain size weighted mean values being, respectively, 0.40 and 0.29 mm). These values were calculated as the weighted average of the screen (or sieve) diameter by the weight of material pinned by the sieve.

The use of sand is due to the weak cohesion strength between grains facilitating an adequate mechanical compaction that determines macroscopic effects on the flux rate. The use of Pyrex cylinders guarantees that neither chemical reactions with water nor crumbling occur. Moreover, because of their dimensions (e.g., cylinder length and diameter of the cylinder are much larger than the sand grain size, cylinder length > cylinder diameter) and their smooth surface, we expect that the porosity range of the Pyrex cylinders medium is much larger than that of the sand and the self-organization of the grains could be sharper. When the mechanical compaction of Pyrex cylinders occurs, the medium may be marked by a moderately compaction to strongly preferred orientation because of the applied head. Homo1, Homo2, and Homo3 are mainly mono-dimensional presenting a characteristic particle size

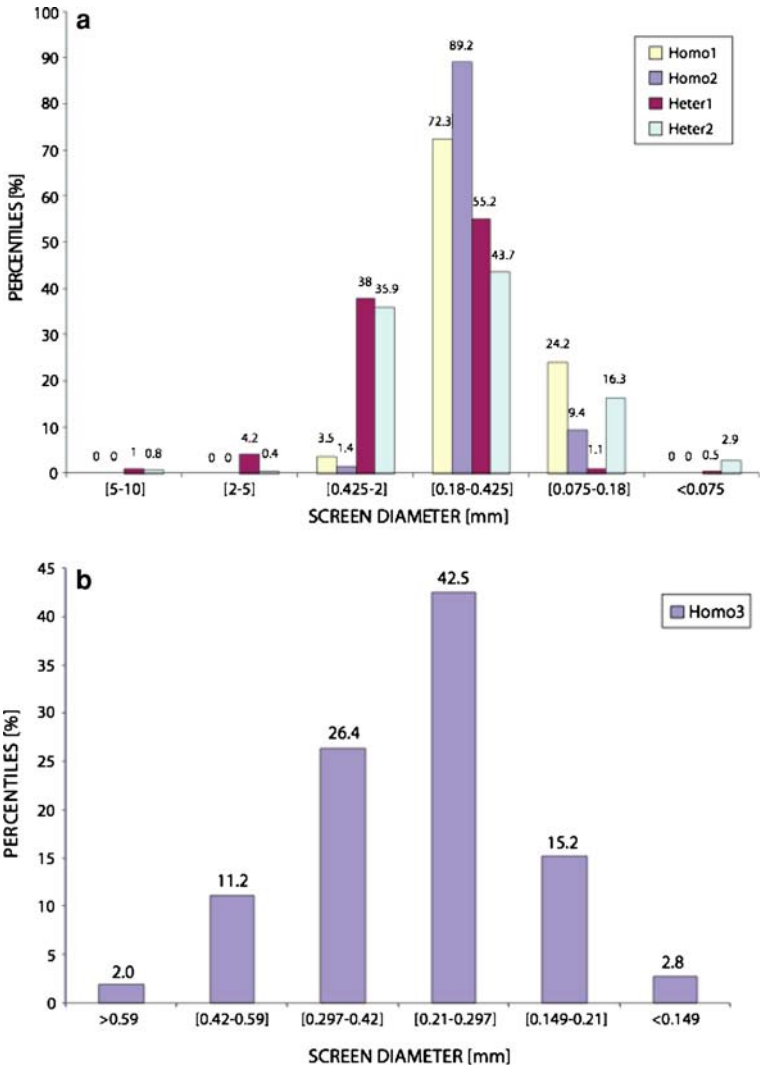

Fig. 2 Bar diagram showing particle size distribution, expressed in terms of percentiles vs. the screen diameter, **a** for porous medium sample of type Homo1, Homo2, Heter1, and Heter2, and **b** for porous medium sample of type Homo3

dimension, while Heter1 and Heter2 are more heterogeneous and should react to mechanical compaction in a different matter than materials characterized by a single characteristic dimension.

In all our experiments, the crumbling of the porous media, e.g., sand, is not expected to occur. In fact, the height of the tank (maximum $h_{\text{tank}} = 2\,\text{m}$) does not provide the extra pressure to be able to crumble the media's grains.

The data set Homo3 is the same as that presented in Iaffaldano et al. (2006) where a memory model for advection in porous media is presented as well, but no asymptotic value for the flux rate is inserted in the parameters to be determined by the minimization procedure. Details of the data monitoring will be presented later.

3.3 Experimental Procedure

In order to perform the experiment, the permeameter was filled with water-saturated sand sample. The saturation was obtained by adding water to dry sand kept in a box. The surplus of water was filtered by means of a very fine mesh fishnet, positioned at one side of the box. Once saturation condition was reached, the cell was filled with sand. In the meanwhile, the position of the tank was set. In order to begin the experiment, tap B is open, and the fluid is allowed to flow through the permeameter from its bottom to the top (Fig. 1).

The flow rate was measured by means of the rotameter with a higher resolution at the beginning of the experiments and less frequently when a constant trend was reached.

In order to guarantee repeatability, many experiments were run under the same hydraulic conditions and using the same kind of medium (experiments labeled C1, C2, Homo1_1, Homo1_2, Homo3_1, Homo3_2, and Homo3_3). The influence of the tank height on both the asymptotic value of the flux and on the memory parameters was tested as well (experiments labeled Homo2_1, Homo2_2, Homo2_3, Heter2_1, Heter2_2, and Heter2_3). Three experiments were run consecutively using the same type of medium by refilling the test section (experiments labeled Heter1_1a, Heter1_1b, and Heter1_1c).

4 Numerical Procedures

A numerical code computes the memory parameters and the fractional order derivative by minimizing the mean of the differences between experimental and theoretical values. The theoretical values of the flux rate at the porous medium upper boundary $q(z = 0, t)$, as a function of time, are computed through (12), where K is the pressure applied at the medium lower boundary, which is due to water filling the constant head tank, and is set equal to $\rho \times g \times h_{\text{tank}}$ where $\rho = 1\text{gr/cm}^3$ is water density, $g = 980.6\text{cm/s}^2$ the acceleration of gravity, and h_{tank} the height of the constant head tank. $q(0, t)$ results a function of integral type depending on time, on the fractional derivative order, and on memory parameters. Equation 12 provides negative values for the flux rate, consistently with the choice of the reference system (the fluid phase diffuses from $z = h$ to $z = 0$). We will deal then with $(-q(0, t))$.

The function to minimize is then

$$SM(n, A, B, D) = \frac{1}{N} \sum_{i=1}^{N} |Dsp_i - q(t_i, n, A, B, D)|$$

where Dsp_i is the i-th flux rate experimentally detected, t_i is the instant of time related to the i-th value, and N is the number of data collected.

In order to simplify the minimization procedure, a given value was assigned to the parameter $A = a/\alpha$ (Caputo 2000): α was set to 1, $a = \rho\psi/\text{K}$ where ρ is the fluid density, ψ is the medium porosity, and K is the bulk modulus ($2.08 \times 10^5 \text{Ncm}^{-2}$ for water) (Domenico and Schwartz 1997). Since A is a function of ψ, two different medium porosities were investigated: $\psi = 0.3$ (providing a value for $A = 1.4 \times 10^{-11}\text{s}^2\text{cm}^{-2}$) and $\psi = 0.1 (A = 5 \times 10^{-12}\text{s}^2\text{cm}^{-2})$. The results show no influence of A on the parameters detected through the minimization procedure. Hence, $q(0, t)$ is now a function of three unknowns $\text{q}(0, t) = q(t, n, B, D)$ where n, B, and D, respectively, range in the domain $[0; 1[\times[0; \infty[\times[0; \infty[$. The domain was further reduced by evaluating the minimum and maximum expected values for all the variables under consideration. n, B, and D have been discretized and a 3-D network of cells of dimensions Δn, ΔB, ΔD was produced. The values of the increments,

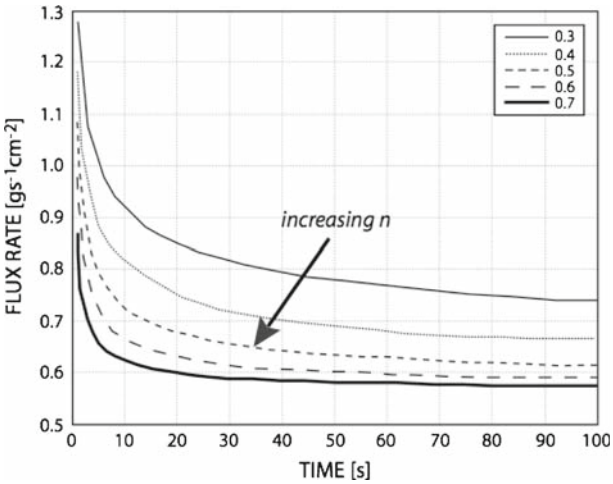

Fig. 3 Flux rate vs. time: n ranges in the interval 0.3–0.7, whereas the other parameters are kept fixed: $A = 1.4 \times 10^{-11}\text{s}^2\text{cm}^{-2}$, $B = 3 \times 10^{-5}$ s, and $D = 5 \times 10^{-5}\text{s}^{1+n}$. *Lines* describe n values {0.3, 0.4, 0.5, 0.6, 0.7}. *Arrow* shows how the studied parameter increases

Δn, ΔB, ΔD, determine the accuracy of the corresponding parameter. Starting from a point within the 3-D network (the point is chosen in a random way), the function $SM(n, B, D)$ is computed at that point and in the 26 adjacent points. The point where the function assumes the lower value is then selected. The same function SM is then computed in all the other points around the one selected. The procedure is repeated until the same point is reached twice. If the point belongs to the boundary of the network, it is a local minimum. In this case, it has to be neglected, since we are interested in an absolute minimum, and the procedure has to be repeated starting from a different point within the network or increasing its dimensions.

The asymptotic value of the flux q_∞, given by

$$q_\infty = \frac{K B}{h} = \frac{\rho g h_{\text{tank}} B}{h}$$

can be used to compute the initial value of B, assuming the asymptotic value is established during the interval of time the experimental data have been acquired.

In order to understand the effect of each of the memory parameters on the theoretical flux rate, one parameter, n, B, or D, was changed each time while the other two are kept fixed.

Figure 3 presents the curves describing the flux rate vs. time for the parameter n ranging in the interval {0.3, 0.4, 0.5, 0.6, 0.7}, B set to 3×10^{-5} s, and D set to $5 \times 10^{-5}\text{s}^{1+n}$. When n increases, the slope of the curve for earlier times increases, and the curve moves downward. Hence, the weights are increasingly smaller with increasing time separation implying that the effect of past is fading with increasing time.

Figure 4 presents the curves describing flux rate vs. time for the parameter B ranging in the interval $\{1, 3, 5, 7, 9\} \times 10^{-5}$ s, $n = 0.5$ and, $D = 5 \times 10^{-5}\text{s}^{1+n}$. With increasing value of B, the function shifts upward.

Figure 5 presents flux rate vs. time for D ranging in the interval $\{1, 3, 5, 7, 9\} \times 10^{-5}\text{s}^{1+n}$, $n = 0.5$, and $B = 3 \times 10^{-5}$ s. When D increases, the slope for early times decreases while all the curves move upward.

It results such that the parameter B plays the role of an additive constant, and its influence on $q(0, t)$, for given values of n and D, is mainly on the second term of Eq. 15, $(-K B/h)$.

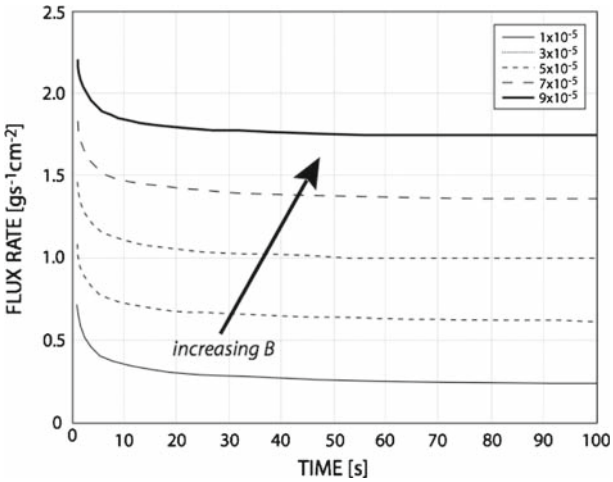

Fig. 4 Flux rate vs. time: B is varied $\{1, 3, 5, 7, 9\} \times 10^{-5}$ s; whereas $A = 1.4 \times 10^{-11} \mathrm{s}^2\mathrm{cm}^{-2}$, $n = 0.5$ and $D = 5 \times 10^{-5} \mathrm{s}^{1+n}$ are constant. *Lines* and *arrow* as in Fig. 3

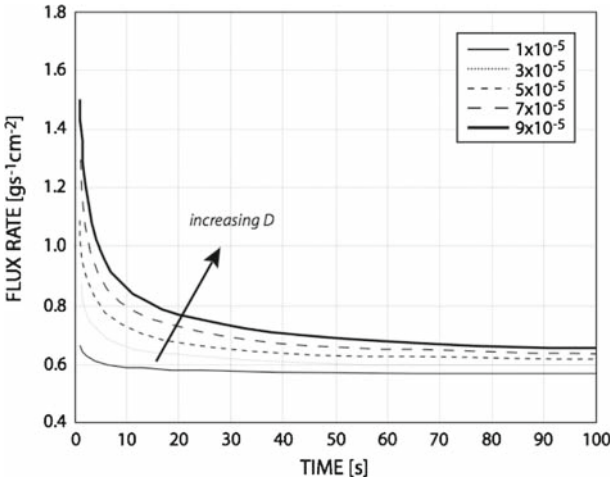

Fig. 5 Flux rate vs. time: D ranges in the interval $\{1, 3, 5, 7, 9\} \times 10^{-5} \mathrm{s}^{1+n}$; while $A = 1.4 \times 10^{-11} \mathrm{s}^2\mathrm{cm}^{-2}$, $n = 0.5$ s and $B = 3 \times 10^{-5}$ s. *Lines* and *arrow* as in Fig. 3

This is confirmed considering the range of variation of B in Fig. 4, $\Delta B = 2 \times 10^{-5}$ s, and the variation of term $-KB/h$:

$$\Delta\left(\frac{KB}{h}\right) = \frac{\rho g h_{\mathrm{tank}}}{h}\Delta B \cong 0.4[gs^{-1}cm^{-2}]$$

where h_{tank} was set to 190 cm. This value is consistent with the distance between curves in Fig. 4.

Equation 12 suggests that the temporal derivative of the flux rate is related to D and n only, where n and D play a similar but opposite effect. In particular, the asymptotic value of the flux rate is reached later for small values of n and large values of D.

5 Observed and Model Results

The following figures show all the experimental data collected. Collection ranges from 1 h to about 10 h depending on the rationale for the experiment. In the first interval of each experiment, a transient phase, where the flux rate decreases, can be recognized. After a time lag depending on the experiment, the flux rate settles to a value lower than the initial one that, in most cases, is close to the asymptotic value. When the steady state is reached, mechanical compaction is over.

Different sets of experiments were carried out to investigate the effects of several parameters, such as the tank height, the grain size of the sand, etc. on the flux rate of the water through a porous medium.

All the collected data are summarized in Table 1. It is not easy to understand from a data set if the asymptotic value for the flux rate is reached. For this reason, the B value from the minimization procedure was used to compute the "theoretical" asymptotic flux rate, $q_{f\,\mathrm{theor}}$. Later on, $q_{f\,\mathrm{theor}}$ value was employed to compute again both the initial, q_i, and final flux ratio, q_f, and the redistribution flux rate ratio to allow a comparison with the results.

5.1 Experiments with Pyrex Cylinders

Two experiments, C1 and C2 (Fig. 6; Table 1), were performed by using Pyrex cylinders. The height of the tank, h_{tank}, was set to 190 cm in both cases. The flow rate was measured for 3.5 h, for every 10 s at the beginning of the experiment, then for every minute and later for every 10 min.

In both experiments, the flux rate decreases during the first half hour and then, it undergoes a smooth increasing that stops after 15 min for C1, and 30 min for C2. After this interval, the flux rate continues to decrease in C1, whereas it reaches an asymptotic value in C2 (Fig. 6).

Table 1 shows that the initial flux, q_i, and the ratio q_i/q_f are larger for C1 than for C2. In addition, the asymptotic value reached during the experiment C1 and the value of the redistribution flux rate ratio, $(q_i - q_f)/q_f$, are higher than the ones reached in C2.

5.2 Experiments with Sand of Type Homo1 and Constant Tank Height

Two experiments, Homo1_1 and Homo1_2 (Fig. 7; Table 1) were conducted under the same experimental conditions with h_{tank} set to 190 cm. The aim of the experiments was to test the repeatability of the experiment under the same operative conditions and to check the effect of different data collection times on the parameters detected through the minimization procedure. Both experiments present a starting value for the flux rate equal to $0.14\,\mathrm{g\,s^{-1}cm^{-2}}$. In the first experiment, Homo1_1, the asymptotic value for the flux rate does not seem to be reached (Fig. 7), while in the second it is reached and is equal to $0.06\,\mathrm{g\,s^{-1}cm^{-2}}$ (Fig. 7; Table 1). Data have been recorded each 10 s at the beginning, 30 s later, 1–10 min at the end. In both cases, the sand within the permeameter presents a significant decrease in height due to mechanical compaction. The intact porous medium sample was extracted in both cases to analyze the macroscopic structure determined by the filtration process. Particles of

Table 1 Summary of the results

Experiment	n	B(s)	$D(\mathrm{s}^{1+n})$	$SM(\mathrm{gs}^{-1}\mathrm{cm}^{-2})$	$q_i(\mathrm{gs}^{-1}\mathrm{cm}^{-2})$	$q_f(\mathrm{gs}^{-1}\mathrm{cm}^{-2})$	q_i/q_f	$(q_i - q_f)/q_f$	h_{tank}(cm)	$q_{f\mathrm{theor}}$	$q_i/q_{f\mathrm{theor}}$	$(q_i - q_{f\mathrm{theor}})/q_{f\mathrm{theor}}$
C1	0.16	1.55×10^{-5}	2.10×10^{-5}	1.15×10^{-2}	0.49	0.33	1.50	0.50	190.0	0.29	1.71	0.71
C2	0.16	1.05×10^{-5}	7.50×10^{-6}	3.24×10^{-3}	0.29	0.22	1.33	0.33	190.0	0.20	1.50	0.50
Homo1_1	0.21	2.00×10^{-6}	8.50×10^{-6}	2.47×10^{-3}	0.14	0.06	2.12	1.12	190.0	0.04	3.68	2.68
Homo1_2	0.21	2.00×10^{-6}	8.50×10^{-6}	2.13×10^{-3}	0.14	0.06	2.40	1.40	190.0	0.04	3.79	2.79
Heter1_1	0.12	5.60×10^{-7}	1.40×10^{-5}	5.70×10^{-3}	0.17	0.07	2.26	1.26	190.0	0.01	16.16	15.16
Heter1_2	0.25	5.20×10^{-6}	1.20×10^{-5}	2.90×10^{-3}	0.18	0.12	1.52	0.52	210.2	0.11	1.72	0.72
Heter1_3	0.21	7.20×10^{-6}	4.40×10^{-6}	3.10×10^{-3}	0.26	0.20	1.31	0.31	262.8	0.19	1.39	0.39
Heter1_1a	0.21	3.40×10^{-6}	1.30×10^{-5}	4.80×10^{-3}	0.17	0.09	1.87	0.87	190.0	0.06	2.66	1.66
Heter1_1b	0.17	3.70×10^{-6}	1.10×10^{-5}	4.70×10^{-3}	0.17	0.10	1.65	0.65	190.0	0.07	2.45	1.45
Heter1_1c	0.15	3.80×10^{-6}	1.00×10^{-5}	3.60×10^{-3}	0.18	0.11	1.58	0.58	190.0	0.07	2.49	1.49
Heter2_1	0.36	3.30×10^{-5}	4.40×10^{-5}	2.26×10^{-3}	0.74	0.65	1.15	0.15	190.0	0.61	1.21	0.21
Heter2_2	0.37	3.20×10^{-5}	7.00×10^{-5}	4.61×10^{-3}	0.94	0.78	1.20	0.20	230.0	0.72	1.30	0.30
Heter2_3	0.35	3.20×10^{-5}	3.90×10^{-5}	6.30×10^{-3}	1.06	0.90	1.17	0.17	270.0	0.85	1.25	0.25
Homo2_1	0.28	3.20×10^{-5}	2.00×10^{-5}	4.90×10^{-3}	0.67	0.63	1.06	0.06	190.0	0.60	1.12	0.12
Homo2_2	0.27	3.30×10^{-5}	2.00×10^{-5}	3.32×10^{-3}	0.88	0.78	1.13	0.13	230.0	0.74	1.19	0.19
Homo2_3	0.26	3.20×10^{-5}	1.80×10^{-5}	5.95×10^{-3}	1.01	0.90	1.12	0.12	270.0	0.85	1.19	0.19
Homo3_1	0.31	1.75×10^{-5}	3.07×10^{-5}	6.23×10^{-3}	0.55	0.39	1.43	0.43	212.0	0.36	1.51	0.51
Homo3_2	0.31	1.75×10^{-5}	4.06×10^{-5}	6.89×10^{-3}	0.58	0.38	1.52	0.52	212.0	0.36	1.59	0.59
Homo3_3	0.34	1.75×10^{-5}	3.73×10^{-5}	6.10×10^{-3}	0.54	0.37	1.43	0.43	212.0	0.36	1.47	0.47

The table shows the name of the experiment, the values of memory parameters, n, B, and D, found with the fitting procedure, the average deviation, SM (i.e., the mean of the difference between experimental and theoretical values modulus), the initial flux rate, q_i, the final flow, q_f, the ratio of the two fluxes, q_i/q_f, the redistribution flux rate ratio, $(q_i - q_f)/q_f$, the height of the tank, h_{tank}, the theoretical final flux, $q_{f\mathrm{theor}}$, the ratio between the initial and the theoretical final fluxes, $q_i/q_{f\mathrm{theor}}$, the theoretical redistribution flux rate ratio, $(q_i - q_{f\mathrm{theor}})/q_{f\mathrm{theor}}$

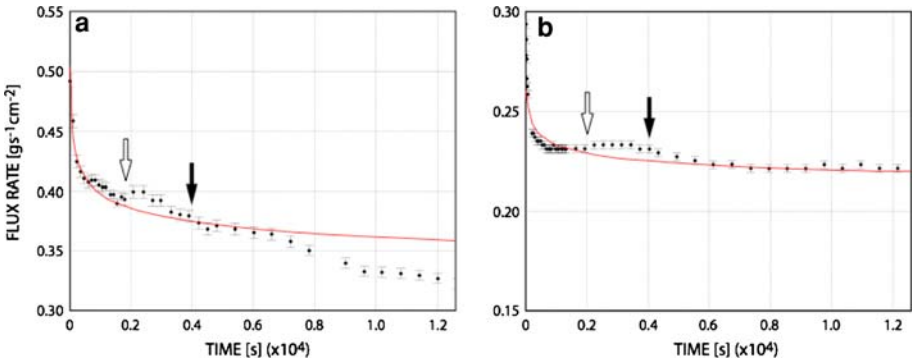

Fig. 6 Flux rate vs. time measured during the experiment C1 and C2 (*black dots*). The *solid line* shows the theoretical flux that best fits the experimental data, where dots represent the experimental flux values. *Arrows* mark the occurring of a macroscopic change in the cylinder distribution. *White arrows* mark the porosity increasing of the medium; *black* one marks the porosity decreasing

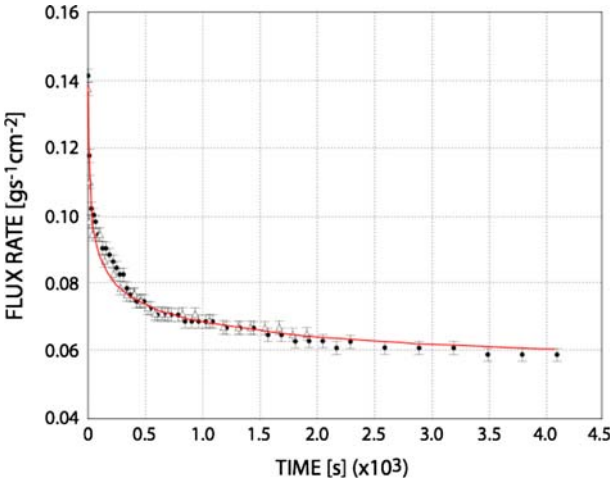

Fig. 7 Flux rate vs. time measured for the Homo1 experiments. *Solid line* as in Fig. 6. *Dots* show Homo1_1 experimental results, triangles Homo1_2 results

small dimensions are confined in the upper part of the matrix, while larger ones are mainly concentrated in the lower boundary of sample.

5.3 Experiments with Sands of Type Homo2, Heter1, and Heter2, and Different Heights of the Tank

The aim of this set of experiments was to test the effect of the tank height and particle size distribution on both the evolution of the flux rate and on the asymptotic value. Three tank heights have been investigated: 190.0, 210.2, and 262.8 cm for medium Heter1 (experiments labeled Heter1_1, Heter1_2, Heter1_3, Fig. 8; Table 1) and 190.0, 230.0, and 270.0 cm for media Heter2 (experiments Heter2_1, Heter2_2, Heter2_3, Fig. 9; Table 1), and Homo2 (experiments Homo2_1, Homo2_2, Homo2_3, Fig. 10; Table 1).

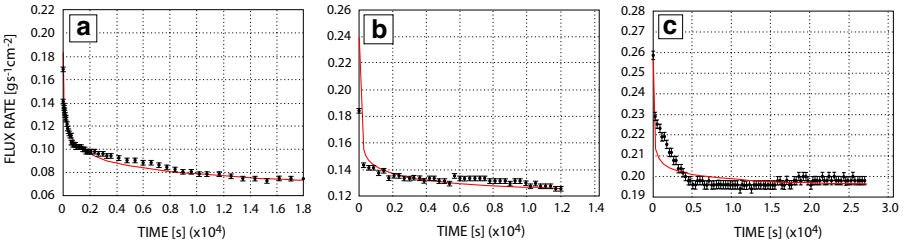

Fig. 8 Flux rate vs. time measured during the Heter1 experiment set. *Solid line* and *black dots* as in Fig. 6

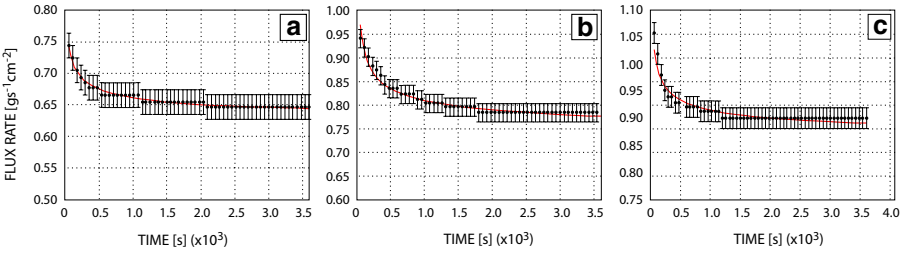

Fig. 9 Flux rate vs. time for the experiments using Heter2 sand type. *Solid line* and *black dots* as in Fig. 6

In the experiments where the medium Heter1 was used (Fig. 8), the flux rate was measured every 10 s during the initial 5 min of each experiment, each minute during 5–15 min, every 5 min during 15–60 min, and every 10 min during 60 min to the end of the experiments. Data have been collected for time periods ranging from 5 h and 30 min (Heter1_1 and Heter1_2) to more than 7 h (Heter1_3). On increasing the tank height, the flux rate ranges between 0.169 $gs^{-1}cm^{-2}$ and 0.074 $gs^{-1}cm^{-2}$, 0.184 $gs^{-1}cm^{-2}$ and 0.121 $gs^{-1}cm^{-2}$, and 0.259 $gs^{-1}cm^{-2}$ and 0.198 $gs^{-1}cm^{-2}$, for h_{tank} equal to 190, 210.2, and 262.8 cm, respectively. With the exception of the experiment with lower h_{tank}, where the flux decreases for the whole run duration (Fig. 8a), in the other two experiments (Fig. 8b, c), the flux rate remains mainly constant during the last 3 h of data monitoring, meaning that the asymptotic regime has been reached (Fig. 8).

The experiments, in which Heter2 sand samples were used, lasted 1 h, and data were collected every 1 min (Fig. 9). With increasing tank height, both initial and final flux rates increase (Table 1). At the same time, q_i/q_f and $(q_i - q_f)/q_f$ measured in the three experiments did not show large differences. Their values are very close to each other (Table 1).

As for the experimental series with Heter2 sand, the experiments carried out with Homo2 sand type lasted 1 h, and measurements were taken every 1 min (Fig. 10). Table 1 shows that the initial and final fluxes have the same behavior as recorded in the previous experiments: q_i and q_f increase with the increasing of h_{tank}, whereas q_i/q_f and $(q_i - q_f)/q_f$ were almost constant (Table 1).

5.4 Experiments with Heter1 and Refilling of the Permeameter

Heter1 sand type was used to perform 3 (Heter1_1a, Heter1_1b, Heter1_1c, Fig. 11; Table 1) consecutive runs (each one lasts approximately 1 h and 10 min) where, in each new experiment, novel sand was placed within the permeameter to fill the empty volume determined by

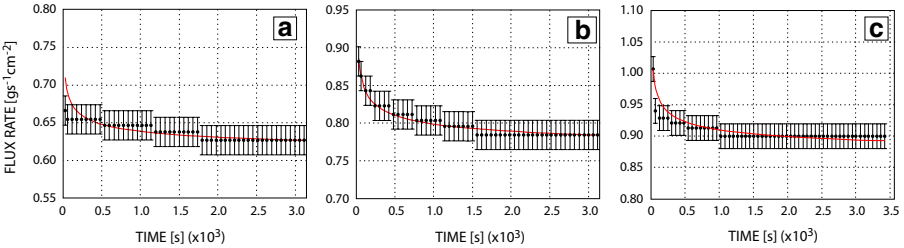

Fig. 10 Flux rate vs. time for experiments performed with Homo2 sand. *Solid line* and *black dots* as in Fig. 6

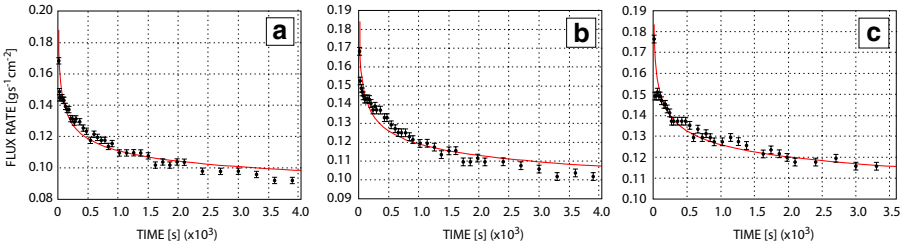

Fig. 11 Flux rate vs. time for the consecutive experiment set carried out by using Heter1 sand. *Solid line* and *black dots* as in Fig. 6

the mechanical compaction occurred in the previous run of the experiment. With increasing volume of porous medium filling the test section, the redistribution of sand particles within the samples was progressively inhibited. The ratio between the initial flux rate and the final one, q_i/q_f, decreases by progressively filling the test section as well as the redistribution flux rate, $(q_i - q_f)/q_f$. The macroscopic structure of the porous sample at the end of the complete set of runs was examined, as was done at the end of the experiments with Homo1 sand. As the Heter1 sand has also particles bigger than those contained in the Homo1 sand, i.e., with diameter of 2–5 mm and even larger than 5 mm (see Fig. 5), the separation between smaller and larger particles is even more evident than that occurred in the experiments performed with the Homo1 sand.

5.5 Experiments with Sands of Type Homo3

Now, three experiments performed under the same experimental conditions, i.e., using the sand Homo3 and h_{tank} set to 212 cm, (Iaffaldano et al. 2006) are shown (Fig. 12; Table 1). The aim of this set of experiments is to test their reproducibility and the repeatability of the numerical procedure to output the same parameters. Measurements of flux rate at the porous medium boundary surface were obtained by storing water in a small container with capacity of about 100 cm^3, and taking note of the relative time interval with a 10^{-2} s precision chronometer. The water mass in the container was measured using a 10^{-4} g precision scale. In order to diminish the error of both the experimenter and the devices, the water mass in each container was measured three times, and each flow measure is the average of three containers filled in rapid succession (more details on the experimental procedure in Iaffaldano et al. 2006).

The flux values, q_i and q_f, were pretty the same for the whole series of runs, as well as q_i/q_f and $(q_i - q_f)/q_f$ values (Table 1).

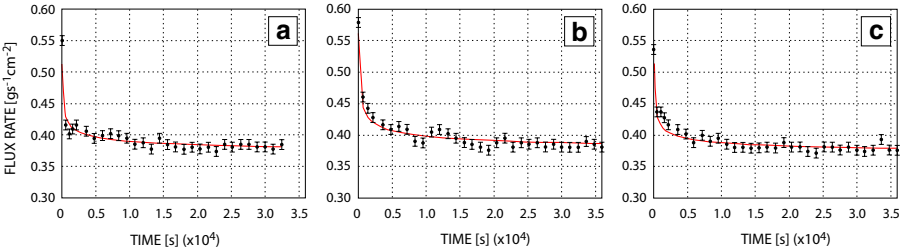

Fig. 12 Flux rate vs. time in the experiments performed with Homo3 sand type. *Solid line* and *black dots* as in Fig. 6

6 Discussion and Conclusions

By comparing our experimental results and the parameters obtained by the minimization procedure, we try to provide information about the influence of the memory, described by memory's parameters, n, B, and D, on the water flux through a porous medium. Memory can be affected by the tank height, the particle size distribution, the stability of the initial particle distribution, etc.

The order of the fractional derivative, n, is a suitable metric for understanding the influence of the memory on the experiments. n ranges between 0.12 and 0.37 (Table 1); thus, this means that the memory largely influences the experiments. At the same time, the parameter D has to be taken into account, because larger values of D imply a stronger influence of memory on the flux rate (Fig. 3). For small values of n and large value of D the asymptotic flux rate will be reached later (Figs. 1 and 3).

Because in geology, especially in rock physics, a great interest is shown in the study of the chemical and mechanical compaction, i.e., rearrangement of the grain, in sands (both coarse, well-sorted and fine-grained ones) and in shales (characterized by elongated shape) (Lash and Blood 2004; Avseht et al. 2005), experiments with sands of different size distribution and pyrex cylinders (par. 4) have been carried out. The composition of the shale is completely different from that of the cylinders, which do not react with water and are not subject to crumbling. Besides, what is occurring at the permeability at high pressure (large depth) and chemical compaction are beyond the scope of this article. Thus, in general, the mechanical compaction of the Pyrex cylinder occurs in the same way, as that occurs with shales.

Two experiments with Pyrex Cylinders have been performed (par. 5). Despite the height of the tank being the same in both experiments, the ratios q_i/q_f are different (q_i/q_f is larger for C1 than for C2, Fig. 6; Table 1), as well as the asymptotic values (the asymptotic value is larger in C2 than in C1, Fig. 6; Table 1). These differences are due to the initial distribution of the cylinders, which is not repeatable, and, consequently, to the initial permeability of the medium. In fact, the range of the cylinder porosity is larger than that of the sand, and the compaction can occur more or less quickly according to the stability of the structure formed by the cylinders. Thereby, during the experiment C2, the asymptotic value of the flux rate is reached faster than in C1, as revealed by both n and D parameters ($n_{C1} = n_{C2}$ and $D_{C1} > D_{C2}$, Table 1), and it is higher for C1 than for C2 ($B_{C1} > B_{C2}$). Observations show that the mechanical compaction occurs in both experiments. The initial distribution of the cylinders in C1 is associated to a larger value of both porosity and permeability (i.e., larger value of the flux rate, Table 1). Accordingly, mechanical compaction occurs following several passages during the experiment C1, as it is evident from the

drops of the flux rate in time. It does not occur in the experiment C2. Despite the same low value of the parameter n, D_{C1} larger than D_{C2} confirms that the medium C1 has a higher memory.

The fitting procedure applied to data recorded during the three experiments that used the Homo3 sand type has produced the same value of B (as expected, the asymptotic flux rate being almost the same, Fig. 12; Table 1). The asymptotic flux rate computed by employing B differs from the value measured by less than 6% confirming that data have been acquired for a time interval sufficient to ensure that the steady state regime is reached. The fitting procedure has produced similar values of $n \in [0.31 \div 0.34]$ and $D \in [3.1 \times 10^{-5} \div 4.1 \times 10^{-5}]$ confirming that the experiments are reproducible, and the minimization search procedure allows obtaining consistent results. Experiment labeled Homo3_2 (Fig. 12b) presents larger value of both q_i/q_f and $(q_i - q_f)/q_f$ (Table 1), i.e., a larger time is required to reach the flux rate asymptotic value, consistently with the smaller value of n and larger value of D.

Experiments, where the tank height was increased and both homogeneous and heterogeneous media have been used, show asymptotic values of the flux rate linearly increasing with increasing h_{tank}. This linear relationship is validated by the constant value of the coefficient B (Table 1). In addition, the memory parameter n is larger for the Heter2 medium with respect to the values obtained in the experiments using more homogeneous media (Table 1). In fact, in a heterogeneous sand, the asymptotic value of the flux rate is reached more quickly than in a homogeneous one. Small grains may jam up between bigger ones, and consequently, the resulting medium configuration becomes steady more quickly than that obtained with a mono-dimensional sand, i.e., Homo2.

Comparing results obtained for homogeneous media, the parameter n increases by increasing the medium average grain size, i.e., for larger grain dimensions, the medium changes its structure faster with a consequent less consistent effect of memory (Fig. 5; Table 1). The parameter D acts in the other way around because it increases with increasing grain size (Table 1).

In the experiments where new sand was added to the medium at the end of each run of the experiment, the measured flux rates present decreasing trends but the increase of the sample density and the correlated decrease of the medium permeability cause the decreasing trend of q_i/q_f. Furthermore, n shows a decreasing trend: memory's action on the medium becomes more important as the sample density increases.

The asymptotic flux computed employing the B value output by the fitting procedure is close to the final flux rate measured experimentally for several but not all the experiments. The experiments where sands of type Homo2, Homo3, and Heter2 have been employed present a final value for the flux rate very close to the asymptotic value. It means that the flux rate was measured long enough ensuring that the steady state regime was reached.

Despite a few assumptions having been employed to perform the fitting procedure, the 3-D numerical code successfully provides an efficient and useful mean to obtain quantitative information about the effects of the memory, expressed by the fractional order derivative, on the experimental flux of water through a porous medium. The very low value of SM (Table 1) validates the model and states that it can be used for investigated phenomena involving memory's effects and water advection. Compressible rocks may be the source of petroleum accumulated in sandstones and carbonates. Determining the behavior of the water flux and the loss of the permeability of a rock it is very important in the investigation of the mechanisms of petroleum migration. Moreover, the variation of the fluid flux depending on the dynamic permeability in seismically active faults may alter their mechanical behavior.

Acknowledgments The authors would like to thank Giampiero Iaffaldano for his suggestions and for providing them with the experimental data. The authors also thank Giovanni Vona and Barbara Muzio for their contribution during the experiments, and Eldred Chimowitz for an interesting discussion.

Appendix

In this appendix, some developments of few equations are added to make the equation reading much easier.

The Laplace operator, LT, is applied to pass from Eqs. 5, 6, and 3 to Eqs. 7, 8, and 9, respectively. When an LT operator is applied to a fractional derivative, the derivative assumes the following expression:

$$\mathrm{LT}[f^{(n)}(t)] = s^n\,\mathrm{F}(s) - s^{n-1}\,\mathrm{F}(0) \tag{A1}$$

where $0 < n < 1$, and s is the Laplace variable. If n is set zero, the LT is

$$\mathrm{LT}[f(t)] = s\,\mathrm{F}(s) - \mathrm{F}(0) \tag{A2}$$

which is the Laplace transform of the first-degree derivative.

Once the governing equations are computed in the Laplace domain, (7–9), they have to be solved to obtain the flux rate through the porous media. Thus, (9) has to be solved in terms of $M(z, s)$:

$$M(z,s) = \frac{1}{s}(m(z,0) - Q_z(z,s)) \tag{A3}$$

Substituting (A3) in (8) we obtain the following expression:

$$(a + bs^{m_1})P(z,s) - bs^{m_1-1}p(z,0) = -\frac{1}{s}(\alpha + \beta s^{m_2})[Q_z - m(z,0)] - \beta s^{m_2-1}m(z,0) \tag{A4}$$

(7) has to be solved in terms of $Q(z, s)$:

$$Q(z,s) = -\frac{(c + ds^{n_2})}{(\gamma + \varepsilon s^{n1})}P_z \tag{A5}$$

and differentiated respect to z:

$$Q_z(z,s) = -\frac{(c + ds^{n_2})}{(\gamma + \varepsilon s^{n1})}P_{zz} \tag{A6}$$

By substituting (A6) in (A4), we find a second-order non-homogeneous differential equation:

$$\frac{(c + ds^{n_2})}{(\gamma + \varepsilon s^{n_1})}P_{zz} = \frac{1}{(\alpha + \beta s^{m_2})}[-\alpha m(z,0) + (a + bs^{m_1})s\,P - bs^{m_1}\,p(z,0)] \tag{A7}$$

Because we assume $n_1 = n_2 = m_1 = m_2 = n$ and $b = \beta = 0$, the Eq. A7 has the following expression:

$$\frac{(c + ds^n)}{\gamma}P_{zz} = \frac{a}{\alpha}s\,P - m(z,0) \tag{A8}$$

Solving (A8) in terms of P_{zz} and, substituting the Eq. 6, that is, $ap(z,t) = \alpha m(z,t)$, we obtain:

$$P_{zz} = \frac{a\gamma}{\alpha(c + ds^n)}[s\,P - p(z,0)] \tag{A9}$$

The solution of this differential Eq. A9 can be written as

$$P(z,s) = D_1(s)e^{zM} + D_2(s)e^{-zM} + \frac{K}{s} \tag{A10}$$

where

$$M = \left[\frac{a\gamma}{\alpha}s(c + ds^n)\right]^{1/2} \tag{A11}$$

$D_1(s)$ and $D_1(s)$ are determined by imposing the boundary conditions in the Laplace domain. They are equal as shown below:

$$D_{1,2}(s) = \mp\frac{K}{s}\frac{e^{\mp hM}}{e^{-hM} - e^{hM}} \tag{A12}$$

The general expression of the Eq. A10, that is

$$P(z,s) = \frac{K}{s}\left[\frac{e^{(z-h)M} - e^{-(z-h)M}}{e^{hM} - e^{-hM}} + 1\right] \tag{A13}$$

has to be differentiated with respect to z and substituted into Eq. A5. The flux rate in the Laplace domain is described in (10).

References

Adolfsson, K., Enelund, M., Olsson, P.: On the fractional order model of viscoelasticity. Mech. Time Depend. Mater. **9**, 15–34 (2005)

Avseht, P., Mukerji, T., Mavko, G.: Quantitative Seismic Interpretation: Applying Rock Physics Tools to Reduce Interpretation Risk. Cambridge University Press, Cambridge, UK (2005)

Bagley, R.L., Torvik, P.J.: On the fractional calculus model of viscoelastic behaviour. J. Rheol. **30**(1), 133–155 (1986)

Bear, J.: Dynamics of Fluids in Porous Media. Dover, New York (1972)

Bell, M.L., Nur, A.: Strength changes due to reservoir-induced pore pressure stresses and application to Lake Oroville. J. Geophys. Res. **83**, 4469–4483 (1978)

Caputo, M.: Elasticitá e dissipazione. Zanichelli, Bologna (1969)

Caputo, M.: Diffusion of fluids in porous media with memory. Geothermics. **28**, 113–130 (1999)

Caputo, M.: Models of flux in porous media with memory. Water Resour. Res. **36**(3), 693–705 (2000)

Caputo, M.: Distributed order differential equations modelling dielectric induction and diffusion. Fractional Calc. Appl. Anal. **4**, 421–442 (2001)

Caputo, M.: Economy Equilibrium Equations with Memory. National Academy of Lincei, Italy (2002)

Caputo, M., Kolari, J.: An analytical model of the Fisher equation with memory function. Altern. Persp. Financ. Account. **1**, 1–16 (2001)

Caputo, M., Mainardi, F.: A new dissipation model based on memory mechanisms. Pure Appl. Geophys. **8**(91), 134–147 (1971)

Caputo, M., Plastino, W.: Diffusion in porous layers with memory. Geophys. J. Int. **158**, 385–396 (2004)

Caputo, M., Plastino, W.: Rigorous time domain responses of polarizable media. Annali di Geofisica **41**(3), 399–407 (1998)

Cesarone, F.: Modello di diffusione con memoria in membrane biologiche. Degree Thesis, University of Rome "La Sapienza" (2002)

Cesarone, F., Caputo, M., Cametti, C.: Memory formalism in the passive diffusion across highly heterogeneous systems. J. Membr. Sci. **250**, 79–84 (2005)

Christensen, R.M.: Theory of Viscoelasticity. 2nd edn. Dover Publications, New York (2003)

Cloot, A., Botha, J.F.: A generalised groundwater flow equation using the concept of non-integer order derivatives. Water SA **32**, 1–7 (2006)

Cushman, J.H.: The Physics of Fluids in Hierarchical Porous Media: Angstroms to Miles. Kluwer Academic Press, Dordrecht (1997)

De Espindola, J.J., daSilva Neto, J.M., Lopes, E.M.O.: A generalised fractional derivative approach to viscoelastic material properties measurement. Appl. Math. Comput. **164**, 493–506 (2005)

Domenico, P.A., Schwartz, F.W.: Physical and Chemical Hydrogeology. Wiley, New York (1997)
Elias, B.P., Hajash, A.: Changes in quartz solubility and porosity due to effective stress: An experimental investigation of pressure solution. Geology **20**, 451–454 (1992)
Iaffaldano, G., Caputo, M., Martino, S.: Experimental and theoretical memory diffusion of water in sand. Hydrol. Earth Syst. Sci. **10**, 93–100 (2006)
Jacquelin, J.: Use of fractional derivatives to express the properties of energy storage phenomena in electrical networks. Laboratoires Alcatel de Marcoussis (1984)
Kaviany, M.: Principles of Heat Transfer in Porous Media. Springer, New York (1995)
Lash, G.G., Blood, D.R.: Origin of shale fabric by mechanical compaction of flocculated clay: evidence from the upper Devonian Rhinestreet shale, Western New York, U.S.A. J. Sedim. Res. **74**, 110–116 (2004)
Le Mehaute, A., Crepy, G.: Introduction to transfer motion in fractal media: the geometry of kinetics. Solid State Ion. **9&10**, 17–30 (1983)
Mainardi, F.: Fractional relaxation-oscillation and fractional diffusion-wave phenomena. Chaos Solitons Fractals **7**, 1461–1477 (1996)
Mainardi, F., Raberto, M., Gorenflo, R., Scalas, E.: Fractional calculus and continuous-time finance II: the waiting-time distribution. Physica A **287**, 468–481 (2000)
Neuman, S.: Eulerian-Langrangian theory of transport in space-time nonstationary velocity-fields—exact nonlocal formalism by conditional moments and weak approximation. Water Resour. Res. **29**(3), 633–645 (1993)
Paradisi, P., Cesari, R., Mainardi, F., Maurizi, A., Tampieri, F.: A generalized Fick's law to describe non-local transport effects. Phys. Chem. Earth **26**, 275–279 (2001)
Podlubny, I.: Fractional Differential Equations. Academic Press, San Diego (1999)
Raileigh, C.B., Healey, J.H., Bredehoeft, J.D.: An experiment in earthquake control at Rangeley, Colorado. Science **191**, 1230–1237 (1976)
Roeloffs, E.A.: Fault stability changes induced beneath a reservoir with cyclic variations in water level. J. Geophys. Res. **93**, 2107–2124 (1988)
Scalas, E., Gorenflo, R., Mainardi, F.: Fractional calculus and continuous-time finance. Physica A **284**, 276–384 (2000)
Scheidegger, A.E.: The Physics of Flow through Porous Media. University of Toronto, Toronto (1960)
Singh, P.P., Cushman, J.H., Maier, D.: Three scale thermomechanical theory for swelling biopolymeric systems. Chem. Eng. Sci. **58**, 4017–4035 (2003)
Singh, P.P., Maier, D., Cushman, J.H., Campanella, O.H.: Effect of viscoelastic relaxation on fluid transport in foods. Part II: Imbibition and drying of seeds. J. Math. Biol. **49**, 1–19 (2004)
Wang, L.: Flows through porous media: a theoretical development at macroscale. Transp. Porous Media **39**, 1–24 (2000)